JOURNAL OF SOLID STATE CHEMISTRY 84, 271–279 (1990)

The Structural Consequences of Charge Disproportionation in Mixed-Valence Iron Oxides. I. The Crystal Structure of $Sr_2LaFe_3O_{8.94}$ at Room Temperature and 50 K

P. D. BATTLE,* T. C. GIBB, AND P. LIGHTFOOT

School of Chemistry, The University of Leeds, Leeds LS2 9JT, England

Received June 13, 1989; in revised form September 20, 1989

The crystal structure of the averaged-valence phase of the rhombohedrally distorted perovskite $Sr_2LaFe_3O_{8.94}$ has been refined from neutron powder diffraction data collected at room temperature (space group $R\bar{3}c$, $a = 5.4712$ Å, $\alpha = 60.09°$). All iron sites are identical. The crystal and magnetic structures of the low-temperature antiferromagnetic phase showing a charge disproportionation have been similarly obtained at 50 K. The crystal structure has been refined in space group $R\bar{3}c$, $a = 5.4580$ Å, $\alpha = 60.19°$; the magnetic structure has been refined in $P\bar{3}m1$ using a model derived from considerations of the exchange interactions between ideal localized electron configurations. The results are interpreted in terms of a charge density wave (CDW) and spin density wave (SDW) propagating along the [111] axis of the crystal and commensurate with the crystal lattice. The apparent absence of a periodic structural distortion (PSD) of the same period as the CDW is surprising, and it is suggested that local variations in the strain field brought about by the disordered arrangement of Sr and La may quench the PSD which would otherwise occur.

Introduction

The cubic perovskite $SrFeO_3$ is a metallic oxide which is antiferromagnetically ordered below 134 K. The iron in this compound can be loosely described as high-spin Fe^{4+}, $3d^4 : t_{2g}^3 e_g^{*1}$, although the high electrical conductivity indicates that the e_g^* orbitals are broadened into an itinerant electron band (*1*). At 4.2 K the Mössbauer spectrum of $SrFeO_3$ consists of a single magnetic hyperfine sextet with a flux density (B) of 33.1 T and an isomer shift (δ) of 0.146 mm s^{-1} (*2*). The spectrum recorded (*3*) for the structurally related material $CaFeO_3$ is very different, showing two sextets of equal area at 4.2 K but with substantially different flux densities and isomer shifts ($B_1 = 41.6$ T, $\delta_1 = 0.34$ mm s^{-1}; $B_2 = 27.9$ T, $\delta_2 = 0.00$ mm s^{-1}). On heating $CaFeO_3$ to 116 K, the two hyperfine fields decrease to zero and the Mössbauer spectrum observed above this temperature consists of two singlets of equal area, which then gradually merge at circa 290 K to form a single line at higher temperatures (*4*). In order to interpret these observations, it was proposed that above 290 K $CaFeO_3$ is a paramagnetic Fe^{4+} oxide, but at lower temperatures the following charge disproportionation begins to take place

$$2Fe^{4+} \rightleftharpoons Fe^{3+} + Fe^{5+}.$$

Between 290 and 116 K the compound was described as a paramagnetic, mixed-valence oxide of Fe^{3+} and Fe^{5+}, becoming an

* To whom correspondence should be addressed.

0022-4596/90 $3.00

antiferromagnetic mixed-valence oxide below the Néel temperature of 116 K (*5*). The charge disproportionation does not take place in $SrFeO_3$, which behaves as an oxide of Fe^{4+} over the whole of the measured temperature range. The mean values of the Mössbauer parameters at 4.2 K reported for $CaFeO_3$ correspond very closely to those reported for the single iron site in $SrFeO_3$.

Subsequently a similar charge disproportionation has been reported in solid solutions including $Sr_{1-x}La_xFeO_3$ and $Ca_{1-x}Sr_xFeO_3$ (*6*). A careful analysis of the available Mössbauer data led Takano *et al.* (*5*) to propose the existence of nonintegral oxidation states in these compounds; that is, the charge disproportionation is more properly written as

$$2Fe^{4+} \rightleftharpoons Fe^{(4-\lambda)+} + Fe^{(4+\lambda)+}, \quad 0 \leq \lambda \leq 1.$$

Part of our own work in this area has focused on the system $Sr_2LaFe_3O_{8+y}$ ($0 \leq y \leq 1$) and the effect of variations in the oxygen content on the charge disproportionation (*7*). This phase differs from $CaFeO_3$ in that the charge disproportionation is from a high-temperature, paramagnetic average-valence state to a low-temperature, antiferromagnetic mixed-valence state; the intermediate paramagnetic mixed-valence state is not observed. We have shown by Mössbauer spectroscopy (*7*) that the transition can be observed in samples having an oxygen content in the range $1 > y > 0.6$; the transition temperature decreases from ~220 to ~180 K as the oxygen content decreases through this range.

Although the phenomenon of charge disproportionation has been recognized in a number of iron oxides, neither the crystal structure nor the magnetic structure of any such low-temperature phase has ever been reported. In this paper we describe a study of $Sr_2LaFe_3O_{8.94}$ by neutron powder diffraction techniques, which have enabled us to determine the crystal and magnetic structures at 50 K. This compound is very close to the ideal stoichiometry $Sr_2LaFe_3O_9$, which would have an average oxidation state of 3.66 for the transition metal cation. The charge disproportionation in the idealized compound can thus be nominally represented as

$$3Fe^{3.66+} \rightleftharpoons 2Fe^{3+} + Fe^{5+}.$$

Our Mössbauer data (*7*) on $Sr_2LaFe_3O_{8.94}$ are consistent with this formulation, comprising a single averaged resonance above 220 K and two magnetic hyperfine sextets below 220 K with area ratios of 69:31 as expected for the stoichiometry of our particular sample. The magnetic transition appears to be locally first-order, but takes place over a range of temperatures in a ceramic powder sample.

We undertook the diffraction study with the expectation of finding both structural and magnetic ordering of the Fe cations at low temperatures. Our results are described below.

Experimental

The preparation, chemical analysis, and X-ray characterization of our sample of $Sr_2LaFe_3O_{8.94}$ have been described previously (*7*). Powder X-ray diffraction measurements indicated a simple cubic perovskite unit cell having $a_0 = 3.874$ Å, although it was noted that the high-angle peaks were somewhat broadened. Neutron powder diffraction data were collected over the angular range $0 < 2\theta < 156°$ on the diffractometer D1a at ILL Grenoble, using a wavelength of 1.909 Å and a 2θ step size of 0.05°. The experiment was performed at room temperature and 50 K using a 10-g sample contained in a vanadium can. Each experiment lasted for ≈11 h.

Results

The neutron diffraction data were analyzed by the Rietveld method (*8*) using the

following coherent scattering lengths: b_{Sr} = 0.69, b_{La} = 0.83, b_{Fe} = 0.95, b_O = 0.58 × 10^{-12} cm. The background level was estimated by interpolation between regions of the profile where there were no Bragg peaks and statistical variations in the background level were taken into account in assigning a weight to each profile point. Data at the lowest angles were excluded from the analysis because of highly asymmetric peak shapes. The lineshape observed at high angles in a powder diffraction experiment is sample dependent and reflects the particle size. During the course of our refinements it became clear that the peaks at higher angles in our data set were symmetric but non-Gaussian and we therefore used a pseudo-Voigt peak-shape in our final calculations (9).

(i) *The Structure of $Sr_2LaFe_3O_{8.94}$ at Room Temperature*

Inspection of the room temperature neutron data showed that the broadening of the high-angle lines in the X-ray diffraction pattern was due to the presence of a small distortion away from cubic symmetry. The neutron data could be indexed in space group $\bar{R}3c$ with a = 5.4712 Å, α = 60.09° or, in the hexagonal setting, a = 5.4784(3), c = 13.3928(4) Å. The latter setting will be used throughout this paper; the $\hat{z}$ axis of the hexagonal unit cell corresponds to the [111] body diagonal of the pseudo-cubic structure. In this space group, the asymmetric unit of the structure consists of three atom sites with a total of only one variable atomic coordinate. The lanthanum and strontium cations were assumed to be fully disordered. Refinement of the usual profile parameters, the atomic coordinate O_x, and the isotropic temperature factors resulted in a weighted profile R-factor of 8.3% (R_{exp} = 2.9%, R_I = 3.0%) for the model described in Table I. The final observed and calculated diffraction profiles are shown in Fig. 1 and bond lengths and bond angles are listed in Table II. No attempt was made to vary the occupation factor of the oxygen atom, which was fixed at unity, because our diffraction experiment is not sensitive to the vacancy concentration of 0.7% predicted by the chemical analysis.

TABLE I

STRUCTURAL PARAMETERS FOR $Sr_2LaFe_3O_{8.94}$ AT ROOM TEMPERATURE (SPACE GROUP $R\bar{3}c$, HEXAGONAL SETTING)

Atom	Site	x	y	z	B_{iso}(Å)
La/Sr	6*a*	0	0	¼	0.72(3)
Fe	6*b*	0	0	0	0.05(2)
O	18*e*	0.5190(2)	0	¼	1.08(3)

Note. a = 5.4784(3), c = 13.3928(4) Å (a_{rhomb} = 5.4712 Å, α_{rhomb} = 60.09°).

(ii) *The Crystal and Magnetic Structures of $Sr_2LaFe_3O_{8.94}$ at 50 K*

Additional scattering, assumed to be of magnetic origin, was apparent in the data set collected at 50 K, which could be indexed in a unit cell smaller (a = 5.4733(2), c = 13.3504(2) Å) than that found at room temperature. Many perovskites adopt a G-type magnetic structure in their antiferromagnetic phase. This ordering arrangement, which gives rise to a characteristic neutron diffraction pattern, has every transition metal cation coupled antiferro-

TABLE II

BOND LENGTHS (IN Å) AND BOND ANGLES (IN DEGREES) FOR $Sr_2LaFe_3O_{8.94}$ AT ROOM TEMPERATURE

Fe–O	1.938(1)	×6	Fe–O–Fe′	173.8
La/Sr–O	2.635(1)	×3	O–Fe–O′	90.16
	2.843(1)	×3		89.84
	2.738(1)	×6		
O–O′	2.745(2)	×4		
	2.738(2)	×4		

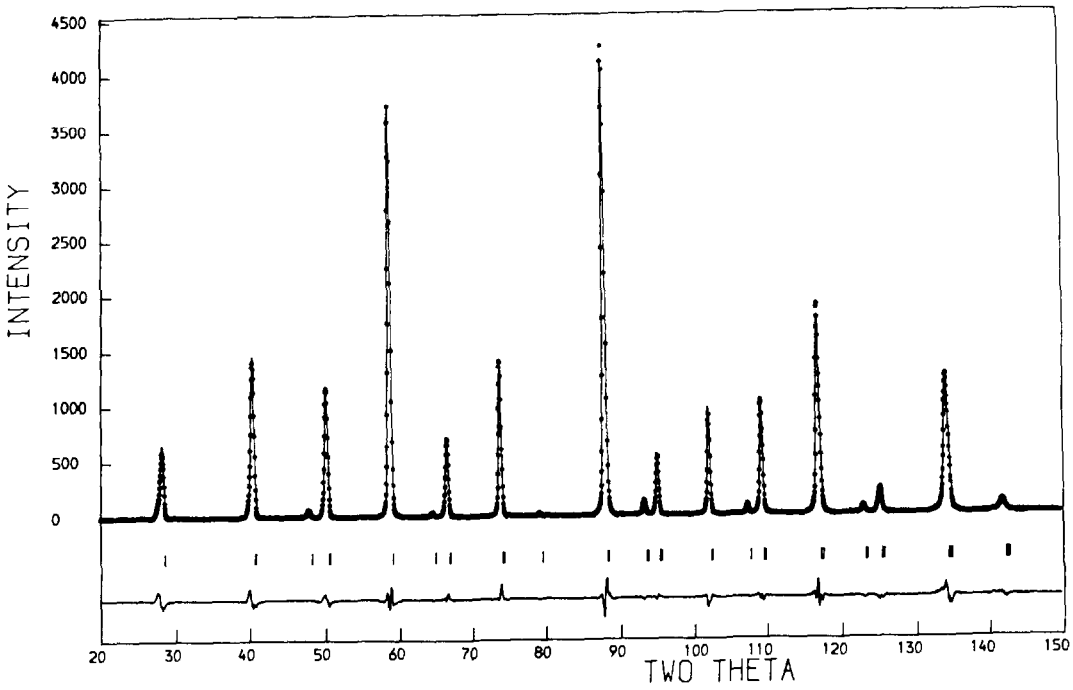

FIG. 1. The observed (···), calculated (—), and difference neutron diffraction profiles for $Sr_2La Fe_3O_{8.94}$ at room temperature.

magnetically to its six nearest neighbors. It was immediately apparent, for example from the presence of a (001) magnetic reflection at $2\theta = 8.2°$, that G-type antiferromagnetism does not occur in $Sr_2LaFe_3O_{8.94}$. The presence of this peak also indicates that the symmetry of the magnetic structure is trigonal rather than rhombohedral and suggests that the ordered magnetic moments lie in the xy plane of the structure rather than along the z axis.

The Mössbauer data for the antiferromagnetic phase are consistent with a 2:1 ratio of the two types of Fe cation with electronic characteristics fairly close to Fe^{3+} and Fe^{5+}, respectively. The two hyperfine sextets are comparatively sharp, suggesting the likelihood of an ordered spin arrangement. In the absence of any other data, an initial model was devised based on reasonable expectations for an idealized localized-electron structure. It has been predicted (*10*) that the superexchange between $Fe^{3+}:3d^5$ and $Fe^{5+}:3d^3$ along a 180° Fe–O–Fe pathway should be ferromagnetic. We therefore attempted to analyze the low-temperature crystal structure in space group $P\bar{3}c1$ using the magnetic model shown in Fig. 2 (the c glide is absent from the magnetic symmetry). This choice of space group allows the ordering of Fe^{3+} and Fe^{5+} over crystallographically distinct sites and the inclusion of ferromagnetic Fe^{3+}–Fe^{5+} superexchange in addition to antiferromagnetic Fe^{3+}–Fe^{3+} coupling. Figure 2 represents layers of Fe^{3+} and Fe^{5+} ions in the sequence . . . 533533 . . . along the $\hat{z}$ axis. The short arrows represent the ordered magnetic moment of an Fe^{5+} ion, the long arrows that of an Fe^{3+} ion. This model accounted for the observed magnetic scattering, but we were unable to achieve a stable refinement of the crystal structure in $P\bar{3}c1$. However, when the crystal symme-

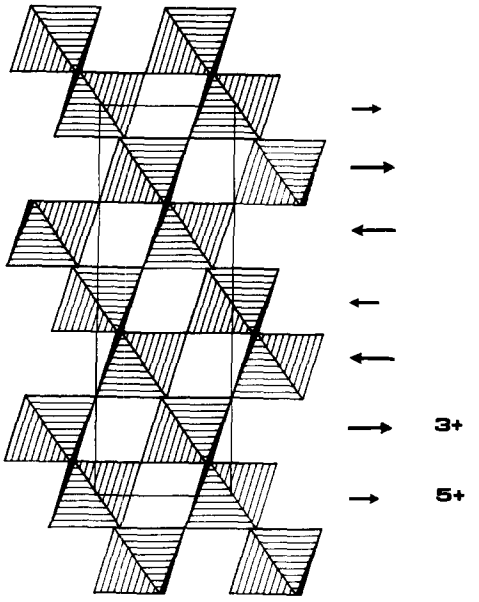

FIG. 2. The FeO_6 octahedra projected onto the (010) plane of the hexagonal setting of the rhombohedral cell. The arrows represent the spin directions from the nominal Fe^{3+} (long arrows) and Fe^{5+} (short arrows) cations.

try was constrained to be $R\bar{3}c$, convergence was reached with $R_{wpr} = 8.8\%$ ($R_{exp} = 2.9\%$, $R_I = 3.5\%$, $R_{mag} = 12.0\%$). We have thus refined the low-temperature structure in a model which permits ordering of the unpaired spin density over two sites but does not permit a concomitant ordering in the crystal structure. The calculated free-ion form factor of Fe^{3+} (*11*) was used to describe the spin density on both iron sites

TABLE III

STRUCTURAL PARAMETERS FOR $Sr_2LaFe_3O_{8.94}$ AT 50 K (SPACE GROUP $R\bar{3}c$, HEXAGONAL SETTING)

Atom	Site	x	y	z	B_{iso}(Å)
La/Sr	6*a*	0	0	$\frac{1}{4}$	0.24(2)
Fe	6*b*	0	0	0	0.16(2)
O	18*e*	0.5266(2)	0	$\frac{1}{4}$	0.50(2)

Note. $a = 5.4733(2)$, $c = 13.3504(2)$ Å ($a_{rhomb} = 5.4580$ Å, $\alpha_{rhomb} = 60.19°$).

TABLE IV

BOND LENGTHS (IN Å) AND BOND ANGLES (IN DEGREES) FOR $Sr_2LaFe_3O_{8.94}$ AT 50 K

Fe–O	1.936(1)	×6	Fe–O–Fe′	171.4
La/Sr–O	2.591(1)	×3	O–Fe–O′	90.32
	2.883(1)	×3		89.68
	2.733(1)	×6		
O–O′	2.748(2)	×4		
	2.733(2)	×4		

in this calculation. The atomic variables in this refinement were the parameter O_x, the isotropic temperature factor of each atom, and the magnetic moments on the Fe^{3+} and Fe^{5+} cations. The latter two parameters refined to 3.61(3) and 2.72(6) μ_B, respectively; the other values are listed in Table III. Bond lengths and bond angles are given in Table IV, and the observed and calculated diffraction profiles are plotted in Fig. 3.

Discussion

The crystal structure of $Sr_2LaFe_3O_{8.94}$ at room temperature is that of a perovskite distorted by a small compression along one of the body-diagonals of the aristotype cubic unit cell. This distortion leaves all the iron–oxygen distances in the FeO_6 octahedra equal, with a value of 1.938 Å. Bond strength/bond length calculations using the method of Brown and Shannon (*12*) indicate that this bond length corresponds to an average valency of 3.66 for the transition metal, in good agreement with the value of 3.63 calculated from the chemical composition. The Sr/La to oxygen distances are all chemically reasonable, as are the oxygen-to-oxygen contacts. The crystal structure at room temperature is thus unremarkable.

The behavior of this compound at 50 K is more interesting. The unit cell is contracted relative to that observed at room temperature, but the oxide ions shift slightly so that the Fe–O bonds retain the same length to

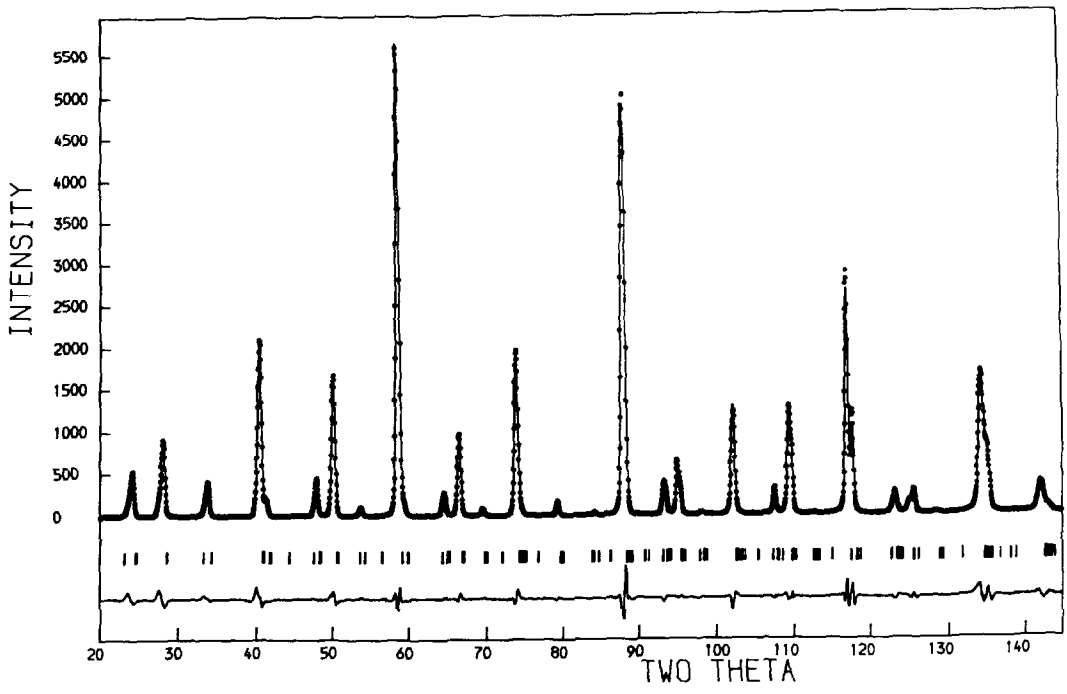

FIG. 3. The observed (···), calculated (—), and difference neutron diffraction profiles for $Sr_2La Fe_3O_{8.94}$ at 50 K.

within experimental error. As a consequence of this, the Fe–O–Fe bond angle, important in determining the nature of the magnetic interactions, decreases from ~174° to 171°. The isotropic temperature factors of all the atoms decrease between room temperature and 50 K, as would be expected in a structure without static structural disorder. Our structure analysis shows that the spin density in this compound is ordered at 50 K, as represented in Fig. 2, with ferromagnetic coupling between nominal Fe^{3+} and Fe^{5+} ions, and antiferromagnetic coupling between pairs of Fe^{3+} ions. In view of the fact that the Fe–O–Fe superexchange pathway is close to linear, this magnetic structure should be regarded as predictable. However, it is possible that the model is not accurate in all details, as it fails to explain the observed field dependence of the susceptibility below 200 K with the implication of some small degree of spin canting.

It is surprising to observe an apparent 2:1 ordering of Fe^{3+} and Fe^{5+} in the magnetic neutron scattering without an accompanying structural distortion. It seems reasonable to expect, in the localized electron limit, that Fe^{5+} cations will occupy smaller octahedral sites than Fe^{3+} cations, but our data indicate that this is not the case; all the transition metal cations have the same environment within the resolution of the experimental data. The explanation must be related to the fact that the charge states are believed to be nonintegral (*5*), and the electrons are at least in part itinerant (it is possible that the t_{2g} electrons are localized and only the e_g^* electrons are itinerant as is thought to be the case in $SrFeO_3$). The observed magnetic moments at the nominal Fe^{3+} and Fe^{5+} sites (3.61 and 2.72 μ_B, re-

TABLE V

MÖSSBAUER PARAMETERS AT 4.2 K FOR IRON IN 6-COORDINATION TO OXYGEN

Compound	Oxidation state	δ(mm s^{-1})	B(T)	Ref.
$Sr_2Fe_2O_5$	+3 localized	+0.50	53.9	*13*
$Ca_2Fe_2O_5$	+3 localized	+0.46	54.7	*13*
$Sr_2LaFe_3O_8$	+3 localized	+0.46	55.5	*13*
$LaFeO_3$	+3 localized	+0.46	56.4	*14*
$SrFeO_3$	+4 itinerant	+0.15	33.1	*1*
$CaFeO_3$	+4 itinerant	+0.34	41.6	*3*
		0.00	27.9	
$Sr_2LaFe_3O_{8.94}$	+3.66 itinerant	+0.35	45.1	*7*
		−0.03	25.9	

spectively) lend support to a model based on the existence of nonintegral charge states in our sample. After allowance for the effects of covalency in the Fe–O bonds, the ordered moment at a 6-coordinate Fe^{3+} cation would be expected to lie between 3.9 and 4.5 μ_B; that at an Fe^{5+} cation might be expected to lie between 2.0 and 2.3 μ_B. The observed moments are thus consistent with a fractional decrease in spin density at the nominal Fe^{3+} site and a corresponding increase at the Fe^{5+} site (any errors in the form factors used in our data analysis are unlikely to be large enough to account for the discrepancy). Strong support for the existence of nonintegral charge states comes from Mössbauer experiments on this and other systems. Table V shows the Mössbauer parameters for a selection of relevant compounds containing iron in 6-coordination to oxygen. If a linear correlation of electron charge and flux density is assumed between $Sr_2Fe_2O_5$ (Fe^{3+}) and $SrFeO_3$ (Fe^{4+}) then the "Fe^{3+}" site in $Sr_2LaFe_3O_{8.94}$ has an actual charge of ca. +3.4 and hence the actual charge of the "Fe^{5+}" site is only ca. +4.2. While these values can only be approximate they are fully consistent with the reduced moments observed in the neutron diffraction experiment. It is also worth remarking that in no case where charge disproportionation has been observed has a quadrupole splitting also been reported. Such a splitting indicates a distorted site symmetry, although the inherent resolution of the Mössbauer technique is poor in this respect, and small distortions might not be detected.

We believe that a realistic description of charge disproportionation in these oxides can be given in terms of a charge density wave (CDW) propagating along $\hat{z}$ in an itinerant electron system. The change from metallic character in $SrFeO_3$ to a semiconductor upon insertion of Ca or La may be merely a manifestation of the well-known Anderson localization which reduces electron mobility in disordered solids, rather than a genuine change to localized electrons. The electron-trapping effects with increasing oxygen vacancy concentration which we reported earlier (*7*) were more compatible with an itinerant electron system.

The low-temperature antiferromagnetic phases can be explained by the simultaneous presence of a spin density wave (SDW). The classic example of a SDW is the antiferromagnetic phase of chromium metal (*15*), which shows a complex spin arrangement, incommensurate with the crystal lattice. However, the introduction of disorder through alloying with other metals can cause a transition to a commensurate

spin system. There is thus an analogy between these alloys and $Sr_2LaFe_3O_{8.94}$ where we observe a commensurate magnetic structure, although $SrFeO_3$, lacking disorder, adopts an incommensurate helical spin system (*16, 17*) which could be described as an SDW. The first-order transition at the Néel temperature of Cr metal is sensitive to defects and strain in the crystal, and a similar dependence may account for the coexistence of two phases near the transition temperature of our ceramic samples of $Sr_2LaFe_3O_{8.94}$.

An SDW may be accompanied by a CDW through electron–phonon interactions, and this in turn should generate a strain wave of the same period, i.e., a periodic structural distortion (PSD) involving atomic displacements. Although in general the CDW is incommensurate, an increasing amplitude of the PSD will favor a pinning of the CDW to some suitable commensurate period, with the charge maxima centered upon the cation sites so as to minimize the strain energies. Such a pinning can also be brought about by the presence of disorder in the crystal structure. It is possible that the variation in the local strain field in $Sr_2LaFe_3O_{8.94}$, brought about by the disordered arrangement of Sr^{2+} and La^{3+} and the oxygen vacancies, may quench the PSD that would otherwise occur in this compound. It seems likely that the surprising occurrence of an apparently commensurate, undistorted structure for $Sr_2LaFe_3O_{8.94}$ is largely due to the presence of disorder on the *A*-site cation sublattice. However, there remains the possibility that the structure is distorted, but by too small an extent to be detected in our neutron experiment. A CDW has been shown to exist (*18*) in the perovskite $BaBiO_3$ where neutron diffraction experiments did detect a small difference in the Bi–O distance in neighboring octahedra (*19*), although XPES (*20*) and calculations (*21*) have shown that the two sites are, electronically, only marginally distinguishable.

We believe that the existence of two nonintegral charge states in $Sr_2LaFe_3O_{8.94}$, as deduced from the Mössbauer data, confirms the existence of a CDW, and the unusual values of the ordered magnetic moments and the flux density are due to a SDW. The neutron diffraction data suggest that both are commensurate with the crystal lattice, and there is no evidence for a PSD. Further structural studies are in progress to throw additional light on this complex problem.

Acknowledgments

We are grateful to the SERC for the award of a postdoctoral research fellowship to P.L. and for the provision of neutron scattering facilities at ILL Grenoble, where we received experimental assistance from Dr. J. K. Cockcroft.

References

1. J. B. MacChesney, R. C. Sherwood, and J. F. Potter, *J. Chem. Phys.* **43,** 1907 (1965).
2. P. K. Gallagher, J. B. MacChesney, and D. N. E. Buchanan, *J. Chem. Phys.* **41,** 2429 (1964).
3. M. Takano, N. Nakanishi, Y. Takeda, S. Naka, and T. Takada, *Mater. Res. Bull.* **12,** 923 (1977).
4. M. Takano, N. Nakanishi, Y. Takeda, and S. Naka, *J. Phys. Colloq. C2* **40,** C2-313 (1979).
5. M. Takano, J. Kawachi, N. Nakanishi, and Y. Takeda, *J. Solid State Chem.* **39,** 75 (1981).
6. Y. Takeda, S. Naka, and M. Takano, *J. Phys. Colloq. C2* **40,** C2-331 (1979).
7. P. D. Battle, T. C. Gibb, and S. Nixon, *J. Solid State Chem.* **77,** 124 (1988).
8. H. M. Rietveld, *J. Appl. Crystallogr.* **2,** 65 (1969).
9. A. D. Murray, A. N. Fitch, and J. K. Cockcroft, unpublished work.
10. J. B. Goodenough, "Magnetism and the Chemical Bond," Interscience, New York (1963).
11. R. E. Watson and A. J. Freeman, *Acta Crystallogr.* **14,** 27 (1961).

12. I. D. BROWN AND R. D. SHANNON, *Acta Crystallogr. Sect. A* **29,** 266 (1973).
13. P. D. BATTLE, T. C. GIBB, AND S. NIXON, *J. Solid State Chem.* **79,** 75 (1989).
14. M. EIBSCHUTZ, S. SHTRIKMAN, AND D. TREVES, *Phys. Rev.* **156,** 562 (1967).
15. E. FAWCETT, *Rev. Mod. Phys.* **60,** 209 (1988).
16. T. TAKEDA, Y. YAMAGUCHI, AND H. WATANABE, *J. Phys. Soc. Japan* **33,** 967 (1972).
17. H. ODA, Y. YAMAGUCHI, H. TAKEI, AND H. WATANABE, *J. Phys. Soc. Japan* **42,** 101 (1977).
18. C. BRUDER, *Physica C* **153–155,** 693 (1988).
19. G. THORNTON AND A. J. JACOBSON, *Acta Crystallogr. Sect. B* **34,** 351 (1978).
20. G. K. WERTHEIM, J. P. REMEIKA, AND D. N. E. BUCHANAN, *Phys. Rev. B* **26,** 2120 (1982).
21. L. F. MATTHEISS AND D. R. HAMANN, *Phys. Rev. B* **28,** 4227 (1983).